Revista EIA

UNIVERSIDAD EIA

Direct Numerical Simulation of Exciton Formation in GaAs Quantum Wells: Effects of Confinement, Donor Impurities and External Magnetic Field

Fabian Andres Castaño[1]
Alvaro Luis Morales[1]
Carlos Alberto Duque[1]

1. Universidad de Antioquia, Colombia

Revista EIA
ISSN 1794-1237
e-ISSN 2463-0950
Año XIX/ Volumen 22/ Edición N.44
Julio - diciembre 2025
Reia4426 pp. 1-31

Publicación científica semestral
Universidad EIA, Envigado, Colombia

Para citar este artículo / To reference this article /
Castaño, F. A.; Morales, A. L. y Duque, C. A.
Direct Numerical Simulation of Exciton Formation in GaAs Quantum Wells: Effects of Confinement, Donor Impurities and External Magnetic Field
Revista EIA, 22(44), Reia4426 pp. 1-31
https://doi.org/10.24050/reia.v22i43.1895

Autor de correspondencia:
Castaño, F. A.
Bioingeniero - PhD en Ingeniería Electrónica y de Computación
Correo electrónico:
fabian.castano@udea.edu.co

Recibido: 26-05-2025
Aceptado:10-06-2025
Disponible online: 01-07-2025

Abstract

We present a numerical study of excitonic states in GaAs quantum wells embedded in $Al_{0.3}Ga_{0.7}As$ barriers, focusing on the effects of quantum confinement and donor impurities. Using a finite element method in cylindrical coordinates, we solve the time-independent Schrödinger equation to obtain electron and hole wavefunctions without assuming trial forms. A parametric sweep of the well thickness from 0.1 nm to 20 nm is conducted to analyze confinement-dependent behavior. The exciton binding energy is computed from the Coulomb interaction integral between spatially resolved wavefunctions. Our results show that confinement enhances energy quantization and modulates excitonic coupling, while the presence of a donor impurity significantly increases wavefunction localization and binding energy. Compared to variational approaches, our method offers higher accuracy and greater flexibility for modeling realistic structures, including impurities and complex boundary conditions. This framework provides detailed insight into exciton formation mechanisms and can be extended to model external fields, strain effects, or more complex heterostructures, offering a valuable tool for the design of next-generation optoelectronic and quantum devices.

Keyword: Excitons; Quantum wells; Finite element method; Binding energy; Donor impurities; GaAs heterostructures.

Simulación Numérica Directa de la Formación de Excitones en Pozos Cuánticos de GaAs: Efectos del Confinamiento, Impurezas Donadoras y Campo Magnético Externo

Resumen

Presentamos un estudio numérico de los estados excitónicos en pozos cuánticos de GaAs incrustados en barreras de $Al_{0.3}Ga_{0.7}As$, enfocado en los efectos del confinamiento cuántico y las impurezas donadoras. Utilizando el método de elementos finitos en coordenadas cilíndricas, resolvemos la ecuación de Schrödinger independiente del tiempo para obtener las funciones de onda del electrón y el hueco sin asumir formas de prueba. Se realiza un barrido paramétrico del grosor del pozo, desde 0.1 nm hasta 20 nm, para analizar el comportamiento dependiente del confinamiento. La energía de enlace del excitón se calcula a partir del integral de interacción de Coulomb entre las funciones de onda espacialmente resueltas. Nuestros resultados muestran que el confinamiento incrementa la cuantización de energía y modula el acoplamiento excitónico, mientras que la presencia de una impureza donadora aumenta significativamente la localización de la función de onda y la energía de enlace. En comparación con enfoques variacionales, nuestro método ofrece mayor precisión y flexibilidad para modelar estructuras realistas, incluyendo impurezas y condiciones de frontera complejas. Este marco proporciona una visión detallada de los mecanismos de formación de excitones y puede extenderse para modelar campos externos, efectos de tensión o heteroestructuras más complejas, ofreciendo una herramienta valiosa para el diseño de la próxima generación de dispositivos optoelectrónicos y cuánticos.

Palabras clave: Excitones; Pozos cuánticos; Método de elementos finitos; Energía de enlace; Impurezas donadoras; Heteroestructuras de GaAs.

1. Introduction

Excitons in semiconductor quantum wells (QWs) are a fundamental subject in condensed matter physics due to their significant role in light–matter interactions and optoelectronic applications. These electron–hole pairs are strongly influenced by quantum confinement, dielectric mismatch, and interface roughness, making them highly

Revista EIA | https://doi.org/10.24050/reia.v22i44.1895

sensitive probes of nanostructure design. In GaAs/AlGaAs systems, excitonic binding energies can surpass those of bulk materials, enabling observable excitonic phenomena even at room temperature (Bastard et al., 1982; Greene et al., 1984). However, a comprehensive understanding of excitonic behavior—especially in the presence of donor impurities and non-ideal geometries—remains incomplete (Bastard et al., 1982; Blancon et al., 2018; Christol et al., 1993; Filinov et al., 2004; Greene et al., 1984).

Theoretical approaches to modeling excitons in QWs range from analytical approximations to full-scale numerical simulations. Variational techniques are widely used for their simplicity and interpretability (Bastard et al., 1982; Greene et al., 1984; Riva et al., 2000). These methods rely on trial wavefunctions to estimate binding energies, making their accuracy sensitive to the chosen ansatz. Despite refinements over time, such as those by Riva et al. (Riva et al., 2000; Zhong et al., 2022), these methods often fail to capture subtle spatial effects and are limited in systems with strong inhomogeneity or complex boundary conditions.

Alternative numerical techniques aim to overcome these limitations. For instance, finite-difference methods (Belov & Khramtsov, 2017) directly discretize the Schrödinger equation, providing detailed insights into the effects of well width and material composition. Belov and Khramtsov (Belov & Khramtsov, 2017) reported binding energies of approximately 13.4 meV for 1 nm QWs. Similarly, fractional-dimensional models (Christol et al., 1993; de Dios-Leyva et al., 1997) incorporate confinement effects into effective dimensionality, offering a semi-empirical approach to estimating binding energies, though these models may lack direct physical correspondence.

Path Integral Monte Carlo (PIMC) methods provide a powerful alternative, capturing fluctuations and correlation effects in quantum wells. Filinov et al. (Filinov et al., 2004) demonstrated how interface disorder affects the binding energies of excitons, trions, and biexcitons in GaAs-based QWs using PIMC. While accurate, these methods are computationally demanding, limiting their use in large-scale parametric studies. Leavitt and Little (Leavitt & Little,

1990) proposed an integration-based simplification that balances computational efficiency with reasonable precision.

Despite the diversity of modeling approaches, a review of recent literature reveals persistent limitations. Of the ten influential studies examined, only two explicitly addressed impurity effects, and only one included a spatially localized donor impurity (Blancon et al., 2018; Filinov et al., 2004; Ghosh et al., 2023). Additionally, most studies confined their analysis to 1D or effective 2D models, ignoring the inherently 3D nature of QWs (Chuu et al., 1994; Gerlach et al., 1998). This simplification restricts the applicability of the results to experimental systems, which often exhibit anisotropic features and asymmetrical interfaces.

A detailed comparison of these studies reveals significant gaps, particularly the lack of analysis on narrow wells, especially those with thicknesses as small as 0.1 nm and with resolution steps as fine as 0.1 nm, extending up to larger well widths. Furthermore, the absence of detailed impurity modeling, particularly regarding donor impurities, is a major shortcoming. This is crucial for accurately capturing excitonic behavior in realistic nanostructures, where unintentional doping, interface defects, and charged traps are almost unavoidable (Belov & Arkhipov, 2023; Filinov et al., 2004; Heckötter et al., 2024).

To address these challenges, we propose a two-dimensional axisymmetric model based on the finite element method, which can be extended to 3D geometries to simulate excitonic states in GaAs/$Al_{0.3}Ga_{0.7}As$ quantum wells. Our approach explicitly incorporates the spatial presence of a donor impurity and resolves the electron and hole wavefunctions directly, without assuming any specific shape. Binding energies are calculated via spatial Coulomb integrals using the resulting wavefunctions. Unlike previous studies that rely on 1D or 2D variational approximations and often overlook impurity effects (Gerlach et al., 1998; Greene et al., 1984; Riva et al., 2000), our method offers full spatial resolution and enables direct analysis of how donor impurity localization affects wavefunction overlap and excitonic binding. By varying the well width across a broad range, we also provide a comprehensive view of the transition from strong to weak confinement—an aspect that has been inconsistently

Revista EIA https://doi.org/10.24050/reia.v22i44.1895

or incompletely addressed in earlier works (Bastard et al., 1982; Gerlach et al., 1998; Yücel et al., 2022). This framework bridges the gap between idealized models and experimental realities, providing a foundation for future studies involving external fields, phonon coupling, or structural asymmetries.

The paper is organized as follows: In Section 2, we outline the theoretical framework, including the governing equations and numerical methods employed. Section 3 presents our results, focusing on the binding energies and wavefunction characteristics across various well widths and impurity configurations. Finally, in Section 4, we summarize our findings and discuss their implications for future research in excitonic systems.

2. Theoretical Background

Understanding the excitonic states in semiconductor heterostructures requires a robust theoretical framework that simultaneously captures the effects of single-particle confinement and the Coulomb interaction between electrons and holes. This is especially challenging in systems like GaAs quantum wells embedded in $Al_{0.3}Ga_{0.7}As$ barriers, where both quantum confinement and impurity effects can significantly alter the excitonic behavior.

2.1. Effective Mass Approximation and Confinement Model with Impurity Interaction

Within the effective mass approximation, the behavior of charge carriers (electrons and holes) confined in a quantum well is governed by a modified Schrödinger equation. Near the band edge, the dispersion relation is approximated as parabolic, allowing the replacement of the actual mass by an effective mass m^*, which accounts for band structure effects. An external static magnetic field $\vec{B}=B_0\,\hat{z}$ is considered, oriented along the growth axis of the quantum well. To incorporate the magnetic field into the quantum description, the canonical momentum $\vec{p}=-i\hbar\nabla$ is replaced according to the minimal coupling prescription:

$$\vec{p} \rightarrow \vec{p} + q_{e/n}\vec{A},$$

where q_e=—e for electrons, q_h=+e for holes, and $\vec{A}$ is the vector potential associated with $\vec{B}$. Here, the symmetric gauge is adopted in cylindrical coordinates (r,ϕ,z), where the vector potential $\vec{A}$ is expressed as:

$$\vec{A} = \frac{B_0}{2} r\hat{\phi},$$

The total Hamiltonian that includes the magnetic field, the confinement potential $V_{e/h}(\vec{r})$, and an impurity potential $V_{imp}(\vec{r})$ modeling a donor impurity placed at r=0 and z=z_{imp} (typically at mid-well) is given by:

$$H_{e/h} = \frac{1}{2m^*_{e/h}}\left(\vec{p} + q_{e/h}\vec{A}\right)^2 + V_{e/h}(\vec{r}) + V_{\text{imp}}(\vec{r}) \quad (1)$$

Here, $V_{e/h}(\vec{r})$ describes the spatial confinement of electrons and holes (see Eq. 2), and $V_{imp}(\vec{r})$ represents the Coulomb interaction between the carriers and the donor impurity located at $\vec{r}_{imp}$ (see Eq. 3). These potentials, together with the effective mass approximation and the inclusion of the magnetic field, define the behavior of charge carriers in the quantum well.

$$V_{e/h}(\vec{r}) = \begin{cases} 0, & \text{inside the GaAs quantum well,} \\ V_0^{e/h}, & \text{within the AlGaAs barrier regions,} \end{cases} \quad (2)$$

$$V_{\text{imp}}(\vec{r}) = -\frac{e^2}{4\pi\varepsilon_0\varepsilon_r\left|\vec{r} - \vec{r}_{imp}\right|}, \quad (3)$$

To numerically solve the Schrödinger equation, the system is modeled in cylindrical coordinates (r,ϕ,z), leveraging the axial symmetry of the problem. Under the presence of a magnetic field, the full time-independent Schrödinger equation for the electron or hole wavefunction $\psi_{e/h}(\vec{r})$, The complete model is given by Eq. 4 and expanded as follows in Eq. 5:

Revista EIA https://doi.org/10.24050/reia.v22i44.1895

$$H_{e/h}\psi_{e/h}(\vec{r}) = E_{e/h}\psi_{e/h}(\vec{r}),$$

$$\frac{1}{2m^*_{e/h}}\left(\vec{p} + q_{e/h}\vec{A}\right)^2 \Psi_{e/h}(\vec{r}) + V_{e/h}(\vec{r})\Psi_{e/h}(\vec{r}) + V_{\text{imp}}(\vec{r})\Psi_{e/h}(\vec{r}) = E_{e/h}\Psi_{e/h}(\vec{r}) \quad (4)$$

$$-\frac{\hbar^2}{2m^*_{e/h}}\nabla^2\psi_{e/h}(\vec{r}) + \frac{q^2_{e/h}B^2_0}{8m^*_{e/h}}r^2\psi_{e/h}(\vec{r}) + V_{e/h}(\vec{r})\psi_{e/h}(\vec{r}) + V_{\text{imp}}(\vec{r})\psi_{e/h}(\vec{r}) = E_{e/h}\psi_{e/h}(\vec{r}) \quad (5)$$

To perform the calculation of excitonic states, the following material parameters were used: effective mass of the electron m^*_e=0.067 m_0 and effective mass of the heavy hole m^*_h=0.600 m_0 in Al0.3Ga0.7As barrier domains; effective mass of the electron m^*_e=0.093 m_0 and effective mass of the heavy hole m^*_h=0.510 m_0 in GaAs quantum well domain; electron rest mass m_0=9.1094×10^{-31} "kg" ; conduction band offset V_0^e=300 meV and valence band offset V_0^h=177 meV; the magnetic induction magnitude B_0=5 "T" ; and the relative dielectric constant of GaAs ε_r=12.9.

Dirichlet boundary conditions $\psi(\vec{r} \to \infty) = 0$) are applied on the outer boundaries to emulate an open structure and prevent unphysical reflections. These infinite domains absorb the decaying parts of the wavefunction, replicating the behavior of an infinite medium surrounding the quantum well.

The donor impurity is located at the position $\vec{r}_{imp}$=(0,z_{mid}), where z_{mid} corresponds to the center of the GaAs well for each case of the parametric sweep.

This framework allows us to study both the "pure" exciton state (when V_{imp} (r,z)=0) and the exciton in the presence of a donor impurity (with V_{imp} (r,z) active), thus providing a comprehensive understanding of the impact of impurity-induced perturbations on excitonic properties.

2.2. Interest Geometry

The simulated geometry is defined in COMSOL using the axisymmetric mode as shown in Figure 1. The design comprises two $Al_{0.3}Ga_{0.7}As$ rectangular barrier $Al_{0.3}Ga_{0.7}As$ barrier extends from to

nm and from to nm. The second barrier has identical dimensions but is displaced along the -axis, effectively sandwiching the GaAs quantum well between the two barriers.

Figure 1. *(a) 2D distribution and (b) 3D visualization of the geometry.*

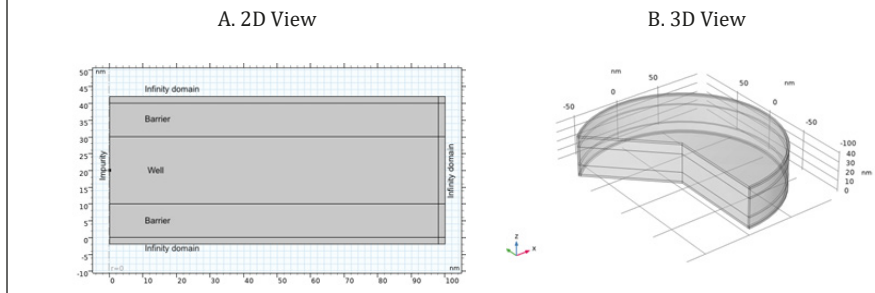

In addition, to simulate excitonic states both with and without a donor impurity, a point impurity is introduced at r = 0 along the z-axis, located in the middle of the GaAs quantum well. This allows for a direct comparison of exciton binding and localization phenomena under pristine conditions versus in the presence of a donor impurity.

The GaAs quantum well is subjected to a parametric sweep in thickness, with the following ranges: from 0.1nm to 5nm in steps of 0.1nm, from 5nm to 20nm in steps of 0.5nm, from 20nm to 50nm in steps of 1nm, and from 50nm to 200nm in steps of 2.5nm along the z-direction. To accurately simulate the effect of a small quantum well embedded in an otherwise infinite material, infinite element boundary conditions are implemented on the bottom, top, and right boundaries of the domain. Dirichlet boundary conditions $\psi_{e/h}(r \vec{} \to \infty)=0$ are applied to the outer boundaries, ensuring that the influence of the infinite surrounding medium on the confined states is adequately taken into account. This approach allows the wavefunction to decay naturally at the edges of the domain, mimicking the behavior of an infinite medium surrounding the quantum well.

A schematic representation of this geometry, including the impurity position, clearly shows the placement of the barriers, the

Revista EIA https://doi.org/10.24050/reia.v22i44.1895

quantum well, and the infinite boundary conditions, providing a comprehensive framework for the simulations (Figure 1).

The geometry was discretized using a uniform square mesh in which all elements had identical size, ensuring consistent spatial resolution throughout the domain. This uniform distribution was precisely fitted to the geometry, achieving a mesh quality (skewness) of 100%. The maximum mesh element size was set to 0.005nm, which guarantees excellent mesh quality and numerical convergence, even for the narrowest well width of 0.1nm. The mesh was generated using COMSOL's built-in meshing tools, which automatically adapt the mesh to the geometry while maintaining the specified maximum element size. This approach ensures that the numerical solution is both accurate and computationally efficient, allowing for reliable simulations across a wide range of well widths.

2.3. Coulomb Interaction and Exciton Formation

Once the confined electron and hole wavefunctions and their corresponding energy levels are obtained, the next step is to evaluate the Coulomb interaction between the two particles. This interaction is responsible for the formation of a bound excitonic state, in which the electron and hole remain correlated due to their mutual electrostatic attraction. The Coulomb interaction energy J is computed as shown in Eq. 6:

$$J = \int_{V_e}\int_{V_h} \frac{e^2}{4\pi\varepsilon_0\varepsilon_r} \frac{\left|\psi_e\left(\vec{r_e}\right)\right|^2\left|\psi_h\left(\vec{r_h}\right)\right|^2}{\left|\vec{r_e}-\vec{r_h}\right|} dV_{\vec{r_h}} dV_{\vec{r_e}} \qquad (6)$$

where e=1.6022×10^{-19} "C" is the elementary charge; ε_0 is the vacuum permittivity; and $\psi_e(\vec{r})$, $\psi_h(\vec{r})$ are the spatial wavefunctions of the electron and the hole, respectively.

$$E_{\text{binding}} = (E_e + E_h) - E_{\text{exciton}}$$

This double integral accounts for the spatial probability distribution of the charge carriers and quantifies their mutual

Coulomb interaction over the entire domain. The calculation is carried out either using COMSOL's built-in integration operators or through post-processing of the exported wavefunctions.

In this framework, the computed interaction energy provides a direct measure of the attractive potential that leads to the formation of a bound excitonic state. However, we emphasize that does not strictly represent the exciton binding energy in the variational sense, where a fully coupled electron–hole wavefunction is employed to obtain the total excitonic ground state energy.

Instead, the true exciton binding energy is defined as the difference between the non-interacting and interacting total energies:

$$E_{\text{binding}} = (E_e + E_h) - E_{\text{exciton}} \tag{7}$$

Where $E_{exciton}$ corresponds to the energy of the coupled excitonic system, as typically obtained from variational or full two-body numerical solutions. In this work, since we compute J using non-interacting wavefunctions, we adopt it as a first-order approximation of $E_{binding}$, with the understanding that this approach neglects excitonic correlation beyond Coulomb overlap.

The evaluation of J across a parametric sweep of quantum well thickness provides valuable insight into how quantum confinement modulates the strength of the exciton interaction, especially in low-dimensional semiconductor systems.

The Coulomb interaction J is computed by evaluating the double integral over the electron and hole wavefunctions, which are defined in three-dimensional space. This integral captures the electrostatic interaction between the charge carriers and is essential for understanding the excitonic binding energy.

The integration is performed over the entire volume of the quantum well and barriers, considering the spatial distribution of the electron and hole wavefunctions. The resulting value of J provides a measure of the strength of the Coulomb interaction, which is crucial for determining the binding energy of the exciton. The exciton

Revista EIA https://doi.org/10.24050/reia.v22i44.1895

binding energy $E_{binding}$ is then calculated as the difference between the total energy of the non-interacting system and the total energy of the interacting system, as shown in Eq. 7. This approach allows us to quantify the impact of quantum confinement and impurity effects on the excitonic properties of the system.

2.4. Comparative Framework Based on Variational Parameters

A well-established theoretical approach to estimating excitonic properties in quantum wells is the use of variational methods. These are especially advantageous when full numerical solutions of the coupled Schrödinger-Poisson system become computationally intensive or analytically intractable. One particularly influential work in this direction is that of Leavitt and Littlejohn (Leavitt & Littlejohn, 2015), which presents a variational formulation of excitons in GaAs/AlGaAs quantum wells by assuming a trial wavefunction that captures the essential geometry and interaction characteristics of the excitonic pair. The trial wavefunction employed in their work is given by Eq. 8:

$$\psi\left(z_e, z_h, \rho\right) = \psi_e\left(z_e\right)\psi_h\left(z_h\right) \cdot \exp\left[-\alpha\sqrt{\rho^2 + \lambda(z_e - z_h)^2}\right] \quad (8)$$

where ρ is the in-plane electron-hole separation, z_e and z_h are the electron and hole coordinates along the growth direction, and α, λ are variational parameters optimized to minimize the total exciton energy. This ansatz approximates the electron-hole correlation while accounting for quantum confinement in the z-direction. In their framework, effective masses and band offsets are held constant, and the quantum wells are treated as symmetric with infinite potential barriers. This simplifies the problem, making it tractable analytically while retaining good physical accuracy for sufficiently wide wells.

To benchmark our fully numerical results obtained through the finite element method (FEM) implemented in COMSOL Multiphysics, we construct a parallel model that replicates the variational assumptions. We adopt the same material constants, band offsets,

and effective masses used by Leavitt and Littlejohn, thereby enabling a direct numerical-versus-variational comparison under identical physical conditions.

3. Results

In this section, the results obtained from the study of the exciton in a GaAs quantum potential well are presented. The energy levels of the individual carriers and the excitonic state are analyzed, both in the presence and absence of a donor impurity. The influence of the well width on the confinement energy and the spatial localization of the carriers is studied, based on the parameters considered in Section 2.1. The results obtained from the numerical solution of the Schrödinger equation for the system under consideration are presented.

3.1. Single-Particle Energy Levels

Figure 2 shows the 15 lowest energy levels for electrons and holes confined in a GaAs quantum well without a donor impurity. As the well width increases, the energy levels shift toward lower values due to the reduction in quantum confinement. This effect is more pronounced for electrons because of their lower effective mass, resulting in larger energy shifts compared to holes. The trend is also observed in the excited states of each particle: as the well width increases, the energy levels become more widely spaced from one another, reflecting the influence of the quantum well geometry on the spacing of quantized states.

Revista EIA https://doi.org/10.24050/reia.v22i44.1895

Figure 2. *Lowest 15 energy levels for electrons and holes in a GaAs quantum well, with and without a donor impurity, in the absence of an external magnetic field. The main plots show the energy levels as a function of the well width, ranging from 0.1 to 200 nm, using a logarithmic scale on the energy axis. Insets display a zoomed view of the 0.1-20 nm range in a linear energy scale to better resolve the behavior of the low-energy states. (A) Electron energy levels without impurity. (B) Hole energy levels without impurity. (C) Electron energy levels with donor impurity. (D) Hole energy levels with donor impurity. In all cases, the lowest energy level corresponds to the particle ground state, while higher levels represent excited states. As the well width increases, the energy levels decrease and the spacing between them becomes smaller, particularly for electrons due to their lower effective mass.*

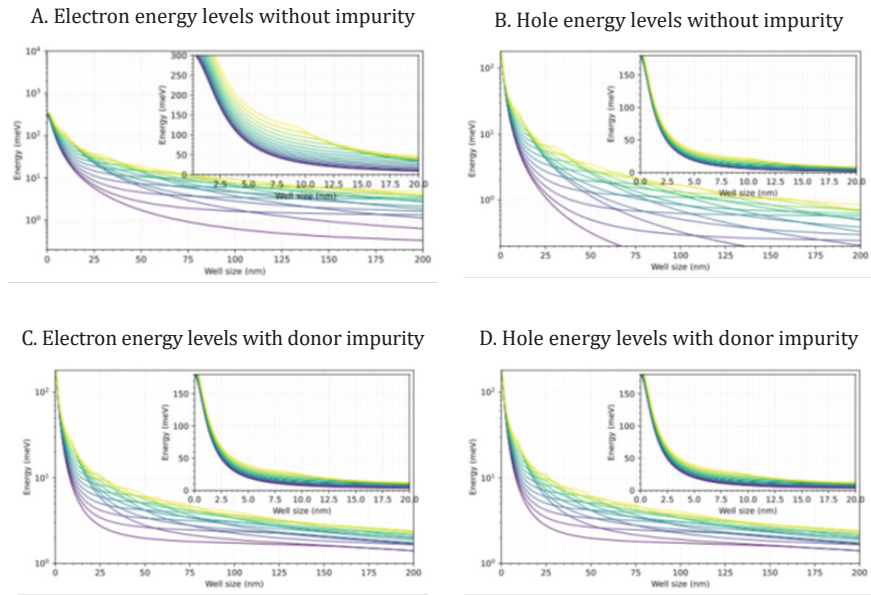

On the other hand, Figure 3 shows the same analysis for the system with a donor impurity placed at the center of the well. The attractive potential introduced by the impurity causes all energy levels to shift downward, indicating stronger carrier localization near the impurity site. This effect is particularly pronounced for the ground state, where the energy level drops significantly compared to the case without impurity. The excited states also exhibit a similar trend, with energy levels becoming more closely spaced as the well width increases. This behavior suggests that the presence of a donor impurity enhances the localization of carriers and alters their energy distribution within the quantum well. The presence of a magnetic field modifies the confinement and leads to energy level splitting, especially visible for narrower wells. The magnetic field affects the energy levels of both electrons and holes, leading to a more complex

energy spectrum. The splitting of energy levels is particularly pronounced for the ground state, where the energy level drops significantly compared to the case without impurity. The excited states also exhibit a similar trend, with energy levels becoming more closely spaced as the well width increases. This behavior suggests that the presence of a donor impurity enhances the localization of carriers and alters their energy distribution within the quantum well.

Figure 3. *Lowest 15 energy levels for electrons and holes in a GaAs quantum well, with and without a donor impurity, under an external magnetic field of 5 T. The main plots show the energy levels as a function of the well width, ranging from 0.1 to 200 nm, using a logarithmic scale on the energy axis. Insets display a zoomed view of the 0.1-20 nm range in a linear energy scale to better resolve the behavior of the low-energy states. (A) Electron energy levels without impurity. (B) Hole energy levels without impurity. (C) Electron energy levels with donor impurity. (D) Hole energy levels with donor impurity. In all cases, the lowest energy level corresponds to the particle ground state, while higher levels represent excited states. The presence of the magnetic field modifies the confinement and leads to energy level splitting, especially visible for narrower wells.*

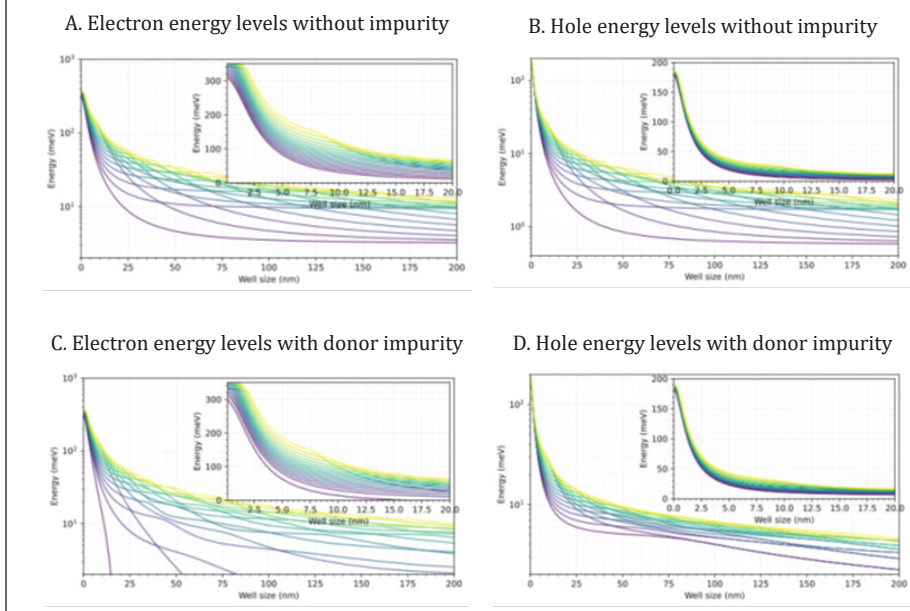

3.2. Estimated Exciton Binding Energy from Coulomb Interaction

The exciton binding energy is estimated using the Coulomb interaction integral between the electron and hole wavefunctions. Figure 4 shows the Coulomb interaction energy , computed using Eq. 6, based on the spatial overlap of the confined electron and hole wavefunctions. Although does not represent the total exciton energy

Revista EIA https://doi.org/10.24050/reia.v22i44.1895

obtained from a fully coupled two-body system, it provides a first-order estimate of the exciton binding energy under the effective mass approximation and independent-particle picture.

Figure 4. Estimated exciton binding energy based on the Coulomb interaction integral as a function of well width, considering different scenarios. (A) Without impurity and without magnetic field. (B) With donor impurity and without magnetic field. (C) Without impurity under an external magnetic field of . (D) With donor impurity under an external magnetic field of . The binding energy is calculated from the Coulomb integral between the electron and hole wavefunctions. The presence of a donor impurity and/or magnetic field modifies the spatial distribution of the wavefunctions, influencing the exciton binding energy.

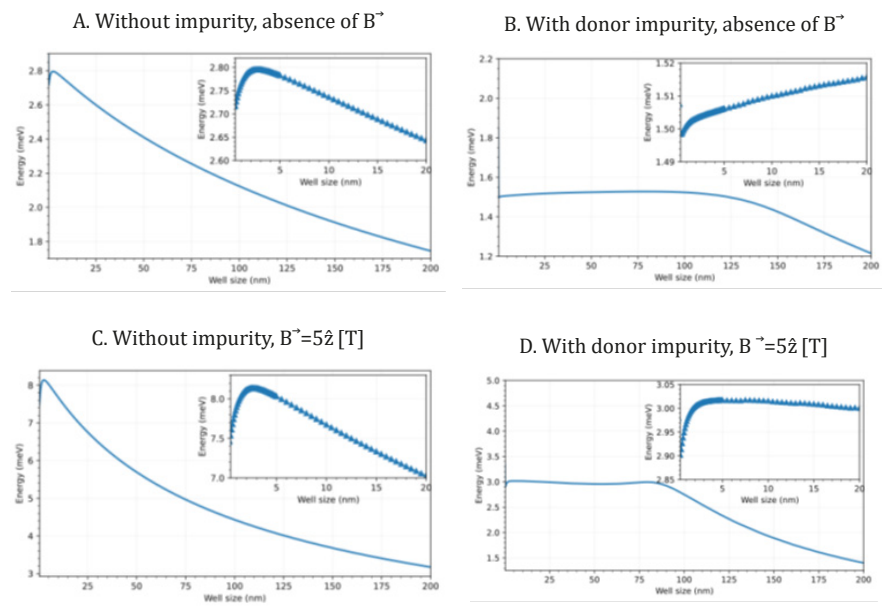

In the absence of both a donor impurity and magnetic field, the Coulomb integral J increases moderately with the well width, reaching a peak value of 2.738 meV at 2.5 nm. This behavior is attributed to the reduced quantum confinement and improved spatial overlap between the electron and hole wavefunctions. However, beyond this point, as the well width continues to increase, the binding energy gradually decreases, reaching 2.702 meV at 20 nm. This decrease is due to the diminishing overlap of the wavefunctions, which leads to a weaker Coulomb interaction. The overall trend indicates that the exciton binding energy is sensitive to the quantum confinement effects, with a maximum value occurring at intermediate well widths.

When a donor impurity is introduced, but still in the absence of a magnetic field, the interaction energy becomes significantly lower. It is observed that the binding energy initially increases with the well width; however, once the well width reaches approximately 100 nm, the electron experiences a confinement energy (E<0) and the hole begins to separate from the electron, causing the binding energy to start decreasing. This reduction arises from the attractive interaction between the electron and the impurity, combined with the repulsive interaction between the hole and the impurity. Such an asymmetric interaction induces a spatial separation between the electron and hole wavefunctions, leading to a decrease in the Coulomb integral due to its inverse dependence on particle separation.

When a magnetic field is applied, both the electron and hole wavefunctions become strongly confined near the center of the quantum well, resulting in a significant increase in their spatial overlap compared to the case without a magnetic field. This enhanced overlap leads to a substantial rise in the exciton binding energy, both in the presence and absence of a donor impurity. In the system without impurity, the binding energy reaches a maximum value of 8.49 “meV” at a well width of 2.5 nm. Beyond this point, the binding energy gradually decreases due to the expansion of the carrier wavefunctions within the wider quantum well, which reduces their overlap.

In contrast, when a donor impurity is present, the interplay between the magnetic confinement and the impurity potential modifies the behavior of the system. Specifically, the magnetic field confines the hole closer to the electron, partially counteracting the repulsive force exerted by the donor impurity on the hole. As a consequence, the binding energy remains relatively stable, around 3.02 “meV” , over a broad range of well widths from 0.1 nm to 90.0 nm. For well widths exceeding 90.0 nm, the hole wavefunction undergoes a symmetry-breaking transition, splitting into two lobes along the z-axis, symmetrically displaced from the impurity position. This spatial separation, driven by the impurity-induced repulsion, diminishes the overlap between the electron and hole wavefunctions, leading to a progressive reduction in the binding energy at larger well widths.

Revista EIA https://doi.org/10.24050/reia.v22i44.1895

3.3. Wavefunction Behavior along the Growth Direction

Figure 5 shows the normalized probability density profiles along the -axis for the value where reaches its maximum. In the absence of an impurity, the wavefunctions for both the electron and hole are more symmetric and delocalized, with both particles localized at nm. As the well width increases, the probability distributions for both the electron and hole spread over a wider range. However, in the presence of a donor impurity, both the electron and hole densities exhibit sharp localization near the center of the well. Specifically, the electron is localized at nm, while the hole is localized at nm. This effect results from the attractive interaction between the electron and the impurity, which causes the electron to be drawn toward the impurity and localize, while the hole experiences a repulsive interaction, causing it to remain more delocalized, albeit still localized near the well center. The presence of the impurity significantly alters the spatial distribution of the wavefunctions, leading to a more pronounced localization of the electron compared to the hole. This behavior is crucial for understanding the dynamics of excitons in quantum wells and their interaction with impurities, which can have significant implications for optoelectronic applications.

Figure 5. *Normalized probability density along the growth direction for the electron and hole with and without donor impurity. (A) Electron without impurity (nm). (B) Hole without impurity (nm). (C) Electron with donor impurity (nm). (D) Hole with donor impurity ((nm)). The presence of the impurity causes the electron to localize near the impurity site, while the hole remains more delocalized but localized near the well center.*

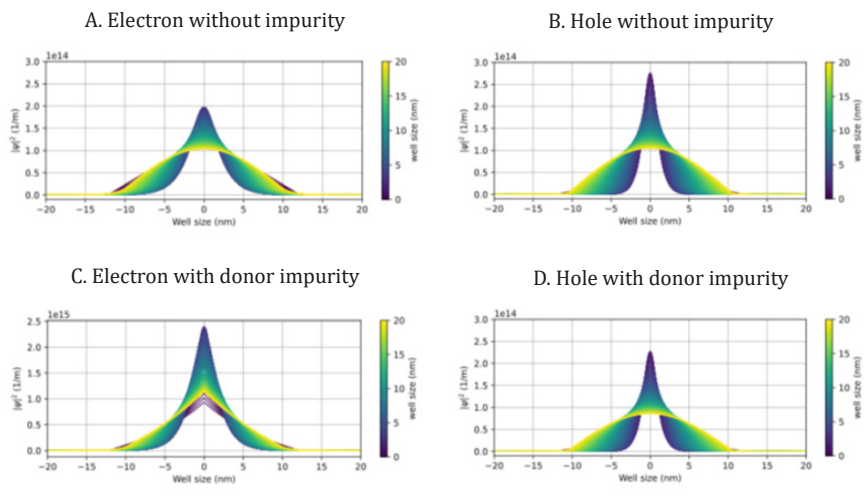

3.4. Magnetic Field Sweep with Donor Impurity

Figure 6 shows how a uniform magnetic field of affects the exciton wavefunction in a GaAs/$Al_{0.3}Ga_{0.7}As$ quantum well with a donor impurity. For well widths , the exciton binding energy remains nearly constant, indicating that both the electron and hole are strongly confined by the combined effect of the quantum well and the magnetic field. However, once exceeds 85 nm, the binding energy begins to decrease. This occurs because, beyond this threshold, the hole and electron separate along the -axis: the donor impurity continues to attract the electron toward , while repelling the hole. The magnetic field still confines both carriers radially, but their axial separation reduces the overlap and thus the Coulomb interaction. This effect is presented in the Figure 6.

Figure 6. *Spatial evolution of the exciton wavefunction in a GaAs quantum well with a donor impurity under a 5 T magnetic field. A marked change in the hole wavefunction occurs between well widths of 50 nm and 100 nm.*

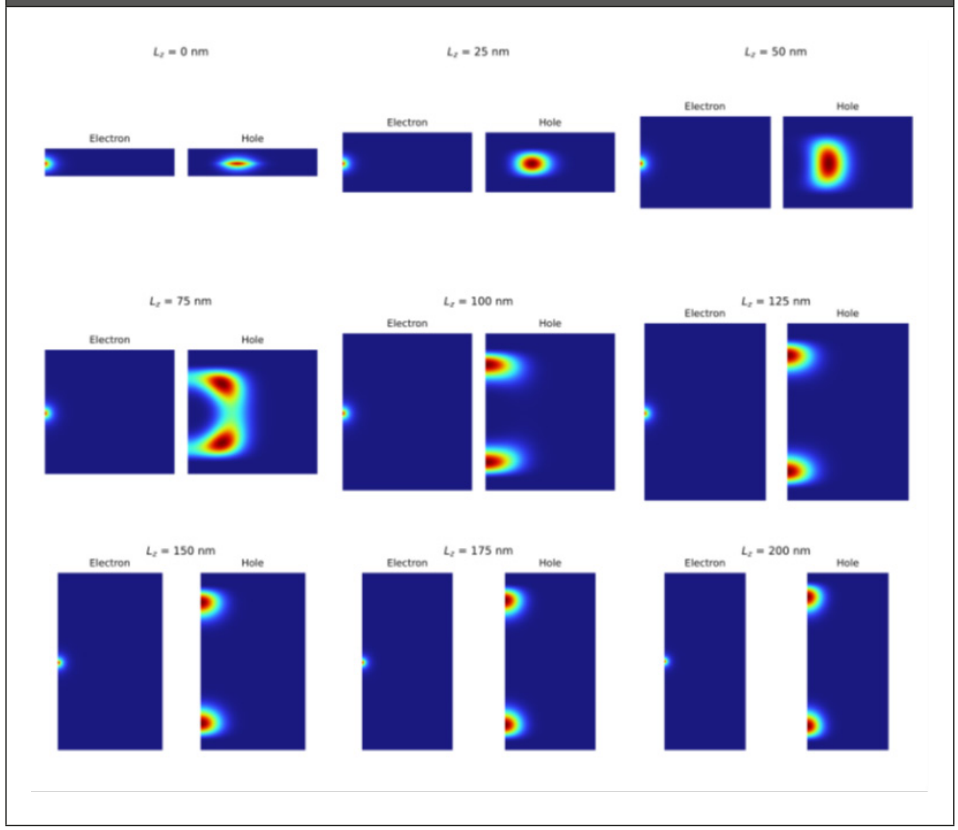

https://doi.org/10.24050/reia.v22i44.1895

To quantify the magnetic-field dependence of the binding energy, we performed a parametric sweep over B=[0, 0.1, 0.5, 1.0, 5.0, 10.0, 15.0, 20.0] T for several well widths. Figure 7 plots the resulting exciton binding energy versus B. For fields below 5 T, the binding energy remains nearly identical to the zero-field, donor-impurity case (Fig. 4B). Beyond 5 T, the binding energy increases: the stronger radial confinement induced by the magnetic field forces the electron and hole closer together in the r-direction, enhancing their overlap. Simultaneously, the splitting of the hole wavefunction occurs at smaller well widths, causing the binding energy to decay more rapidly with L_z. The result of this analysis is shown in Figure 7.

Figure 7. *Exciton binding energy as a function of magnetic field strength for various well widths. The binding energy remains flat below 5 T, then increases due to enhanced radial confinement, and finally decreases with well width as axial separation sets in.*

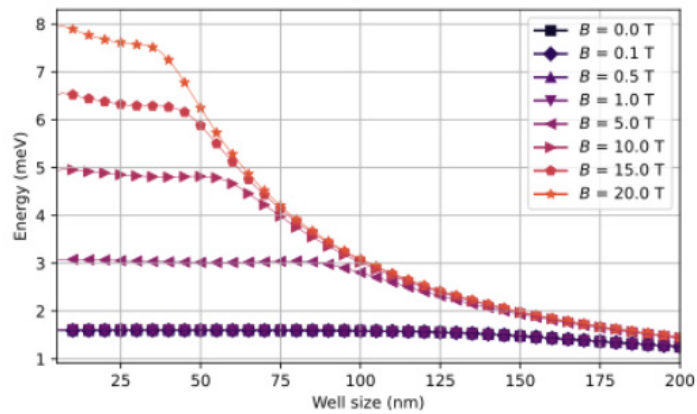

3.5. Exciton Wavefunction Evolution

Figures 8 and 9 show the 2D spatial evolution of the exciton wavefunction for selected well widths, illustrating how the excitonic probability density distribution changes with varying quantum confinement. In the absence of a donor impurity, the exciton wavefunction extends over a broader region of the quantum well, indicating weaker binding and greater delocalization. Conversely, when a donor impurity is present, the exciton becomes strongly localized near the well center, highlighting the enhanced Coulomb attraction between the electron and the impurity.

3.6. Variational Method Comparison

In this section, we compare the results obtained using the variational method with those derived from the direct numerical solution implemented in COMSOL. The variational approach provides a semi-analytical framework for estimating key excitonic quantities such as the Coulomb integral J and the exciton binding energy E_{exc}, based on a parameterized trial wavefunction.

Figure 8. *Spatial evolution of the exciton wavefunction in a GaAs quantum well without a donor impurity. The wavefunction becomes more delocalized as the well width increases.*

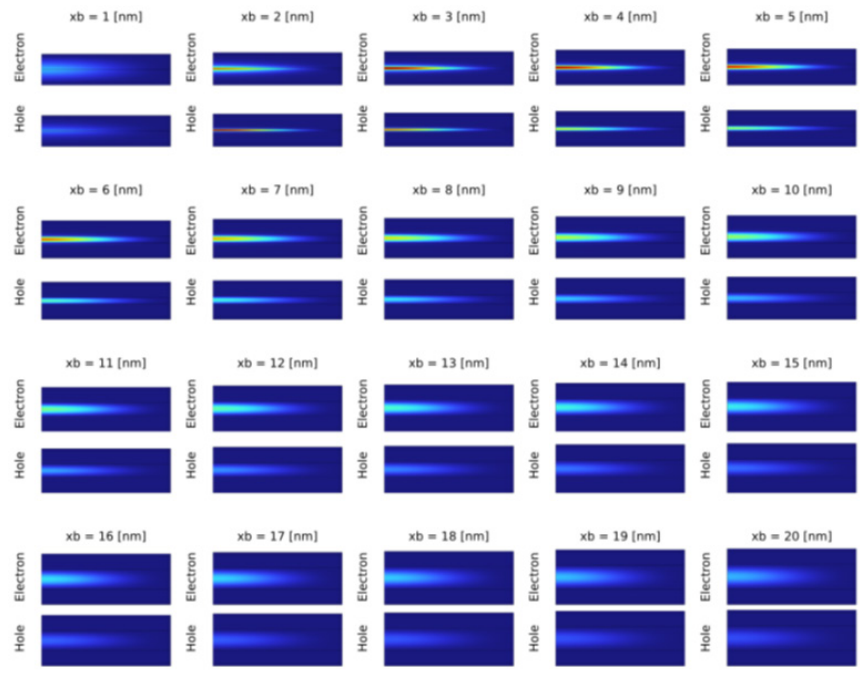

We implemented the variational method independently in Python, employing a nonlinear optimization algorithm to minimize the total exciton energy with respect to the variational parameters α and λ. This dual-method strategy serves both as a consistency check and as a means to understand the differences arising from physical assumptions. While the variational method is limited by idealized conditions (e.g., infinite barriers and isotropic effective masses), the COMSOL-based finite element model includes more realistic features such as finite barrier heights and spatially varying effective masses.

Revista EIA https://doi.org/10.24050/reia.v22i44.1895

Figure 9. *Spatial evolution of the exciton wavefunction in a GaAs quantum well with a donor impurity. The wavefunction remains tightly confined near the impurity site across all well widths.*

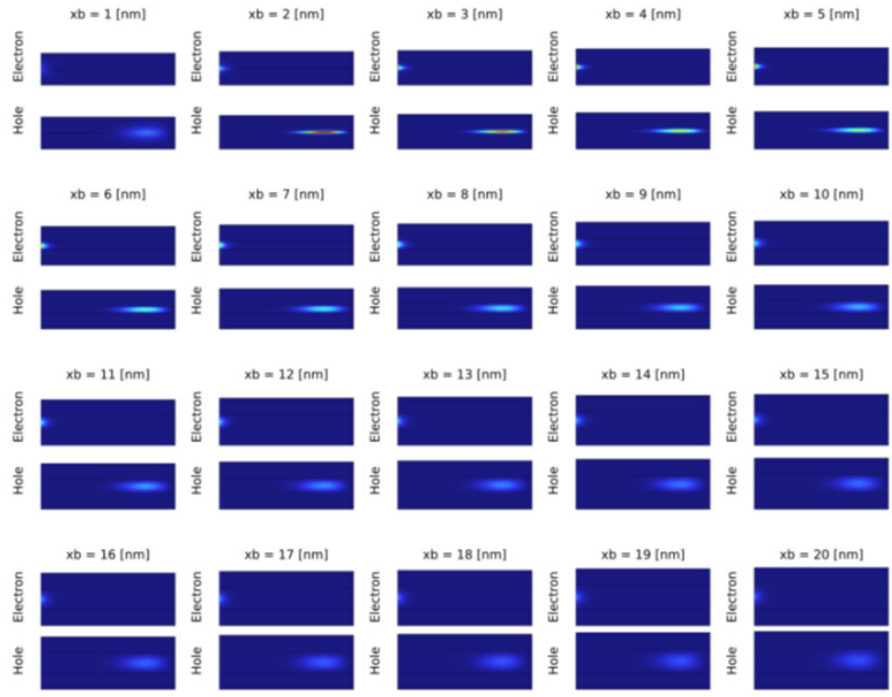

To benchmark our model, we also compared the numerically obtained exciton binding energy with the analytical approximation reported by Leavitt and Littlejohn (Leavitt & Littlejohn, 2015). Their empirical expression for the exciton binding energy , in meV, as a function of quantum well width , is given by:

$$R_x(L) = \frac{3.5431L^2 + 146.694L}{L^2 + 11.1758L + 6.0473}, \quad 1 \leq L \leq 150\text{nm}.$$

This formula achieves a maximum error of 0.07 meV over the specified domain and asymptotically approaches the bulk exciton limit as L to 200 nm. For example, at L=10 nm, the predicted binding energy is approximately 10.8 meV, which is considerably higher than the Coulomb integral J≈2.8 meV computed in our COMSOL model under similar conditions.

This discrepancy is expected, as our Coulomb-based model treats the exciton as two non-interacting, independently confined particles

and neglects explicit wavefunction coupling. Variational methods, on the other hand, include spatial electron–hole correlation, allowing for energy minimization through joint carrier reorganization. This difference is illustrated in Fig. 10, which compares the exciton binding energy computed via the variational method and our COMSOL-based Coulomb model. As such, variational estimates tend to overestimate binding energy, while our model yields a lower bound estimate.

Figure 10. *Comparison of the exciton binding energy obtained using the variational method (Leavitt & Littlejohn, 2015) and the Coulomb interaction calculated via COMSOL simulations.*

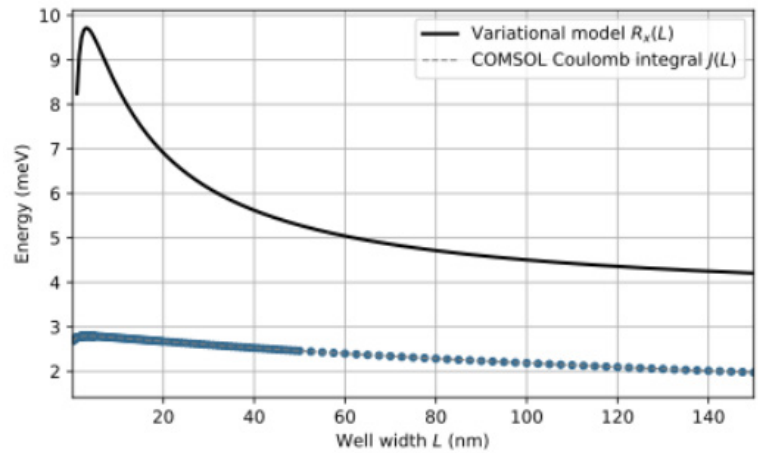

Nevertheless, the trends observed in our simulations qualitatively match those of the variational approach: the Coulomb interaction increases with well width and is further enhanced in the presence of donor impurities. Thus, the computed Coulomb integral serves as a physically meaningful and computationally efficient indicator of excitonic coupling strength across a wide range of heterostructure configurations.

The values of J(L) obtained in this study span from approximately 2.8 meV at L = 3 nm to about 1.8 meV at L = 200 nm, peaking in the transition regime between strong and weak confinement. These values remain lower than those predicted by variational models, which estimate 10.8 meV at L = 10 nm and converge to 4.1 meV for large well widths (Leavitt & Littlejohn, 2015). Figure 11 shows

Revista EIA https://doi.org/10.24050/reia.v22i44.1895

the computed Coulomb integral J over a wide range of well widths, highlighting the peak in the transition region.

These differences arise because the variational method models the correlated motion of the electron–hole pair via a coupled wavefunction, while our COMSOL approach treats the Coulomb interaction as a perturbation on independently computed charge distributions. Thus, the Coulomb integral J provides a conservative, yet robust estimate of the minimum exciton binding energy.

Figure 11. *Coulomb integral computed via COMSOL simulations from 0.1 to 200 nm well width, using material parameters consistent with Ref. (Leavitt & Littlejohn, 2015).*

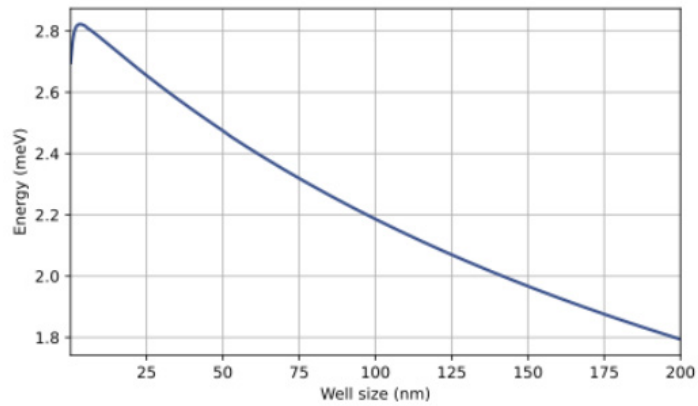

Table 1 summarizes a direct comparison of key parameters between our FEM-based model and the variational reference for a quantum well width of nm. Despite using the same material parameters, discrepancies in quantities like the Coulomb integral are apparent, reflecting the enhanced realism captured by the finite element method.

Table 1. *Comparison between the COMSOL model (using variational parameters) and the reference results reported by Leavitt and Littlejohn (Leavitt & Littlejohn, 2015) for nm.*

Quantity	FEM Model (This Work)	Ref. [11]
Electron mass m^*_e (m_0)	0.067	0.067
Hole mass m^*_h(m_0)	0.155 (avg.)	0.377 (z), 0.111 (xy)
V_e (Conduction offset, meV)	237.6	237.6
V_h (Valence offset, meV)	127.9	127.9
ε_r (dielectric constant)	12.53	12.53
E_e (Electron level, meV)	144.2	149.6
E_h (Hole level, meV)	21.4	21.1
J (Coulomb integral, meV)	2.75	10.8

Additionally, Table 2 provides a qualitative comparison between the variational method and the finite element method, highlighting differences in physical modeling capabilities, implementation complexity, and computational cost. While the variational method is fast and intuitive for preliminary estimates, FEM provides richer spatial insight and greater flexibility for simulating real-world device structures.

Table 2. Comparison between the variational and direct numerical methods used in this study.

Aspect	Variational Method	Finite Element Method (FEM)
Wavefunction	Trial function with variational parameters	Solved from the Schrödinger equation numerically
Accuracy	Depends on trial function choice	Depends on mesh resolution and solver settings
Coulomb Integral	Approximate analytical evaluation	Numerical integration of charge densities
Geometries	Simple and idealized	Arbitrary, including complex or asymmetric domains
Impurities	Requires analytical modeling	Included via spatially varying potentials
Computational Cost	Low	Moderate to high
Physical Insight	Good for qualitative trends	Provides spatially resolved physical insight

Revista EIA https://doi.org/10.24050/reia.v22i44.1895

4. Discussion

Traditionally, excitonic states in semiconductor quantum wells have been studied using variational methods, where a trial wavefunction is proposed and optimized to minimize the total energy of the system. These methods are analytically elegant and computationally efficient, especially for idealized geometries. However, the accuracy of the variational approach depends strongly on the choice of the trial function and its ability to represent the spatial distribution and correlation of the electron–hole pair. This limitation becomes more pronounced in the presence of perturbations such as impurities, structural asymmetries, or nonuniform material parameters (Christol et al., 1993; Leavitt & Little, 1990; Riva et al., 2000; F. Wang et al., 2015).

In this work, we employed a direct numerical solution of the Schrödinger equation using the finite element method in cylindrical coordinates. This approach avoids assumptions regarding the shape of the wavefunction and enables the inclusion of realistic potential profiles, spatially varying effective masses, and boundary conditions (Bastard et al., 1982; Gerlach et al., 1998). As a result, both the electron and hole wavefunctions are obtained independently, and the Coulomb interaction energy is computed using their actual probability densities. Although this introduces an approximation by neglecting direct electron–hole correlation during the wavefunction computation, the method provides a physically transparent and computationally tractable way to evaluate the exciton binding energy in weakly coupled regimes (Belov & Khramtsov, 2017; de Dios-Leyva et al., 1997; Huang et al., 2016; G. Wang et al., 2015).

The advantages of the numerical approach are particularly evident when analyzing donor-impurity effects. In variational formulations, incorporating the impurity potential typically requires a modified or composite trial function, often increasing the model complexity and reducing generality. In contrast, the method used here integrates the impurity directly into the Hamiltonian as a perturbative potential, allowing for a straightforward and precise

treatment of its effect on carrier localization and binding energy (Filinov et al., 2004; Greene et al., 1984). This results in spatially resolved wavefunctions that reveal the degree of localization induced by the impurity and its influence on the electron–hole interaction.

To validate our numerical model, we reproduced the conditions for a GaAs/$Al_{0.3}Ga_{0.7}As$ quantum well with a width of nm. Under these conditions, the variational model predicted an exciton binding energy of approximately 18.7 meV, with a Coulomb interaction energy of meV. In contrast, our model yielded a Coulomb energy of approximately 2.8 meV. This difference stems from the fact that our approach does not consider full electron–hole correlation during the solution of the Schrödinger equation. While the variational method accounts for this by optimizing a correlated trial wavefunction, our approach computes the interaction post hoc, using independent wavefunctions (Chuu et al., 1994; Leavitt & Little, 1990).

Despite this underestimation of the total binding energy, our results qualitatively capture the key physical dependencies: confinement enhances single-particle energies but reduces spatial overlap, and the introduction of a donor impurity significantly increases the Coulomb interaction and exciton binding. These trends align with theoretical predictions and experimental observations (Christol et al., 1993; Leavitt & Little, 1990; Riva et al., 2000).

The flexibility of the finite element method also allows this approach to be extended to more complex scenarios, such as systems under external fields, quantum dots, or coupled quantum wells. Moreover, the method is suitable for modeling carrier dynamics in optoelectronic applications, including quantum cascade lasers, single-photon sources, or excitonic transistors (Belov & Khramtsov, 2017; Ferreira & Bastard, 1997; Greene et al., 1984).

In particular, our parametric sweep of the magnetic field revealed a non-trivial dependence of the exciton binding energy on both field strength and well width (Figure 7). For , the binding energy remains essentially unchanged, mirroring the impurity-only case. Above 5 T, however, stronger radial confinement pulls the electron and hole closer in the r-direction—enhancing —while axial separation eventually reduces overlap for nm. This competition leads to a peak

Revista EIA https://doi.org/10.24050/reia.v22i44.1895

in around 5–10 T and a subsequent downturn at larger widths, consistent with magneto-exciton theory in quantum wells (Bauer & Ando, 1988; Jakubczyk et al., 2016; Turner et al., 2012). The magnetic-field sweep not only confirms the robustness of our FEM framework under external perturbations, but also uncovers a tunable regime in which moderate fields maximize binding before geometric separation dominates.

In summary, the numerical methodology presented here offers a robust alternative to traditional variational techniques, particularly when investigating systems with localized perturbations or complex geometries. While future work may incorporate correlated two-body wavefunctions or hybrid methods to improve quantitative agreement with variational results, the current model provides a solid foundation for studying exciton physics in semiconductor nanostructures with high fidelity and physical insight (Christol et al., 1993; Grandjean et al., 1999; Leavitt & Little, 1990; Riva et al., 2000).

Finally, future work could explore several avenues to further refine and extend the current model. One direction would be to incorporate fully coupled electron-hole wavefunctions, which would allow for a more accurate treatment of the exciton binding energy and Coulomb interaction, particularly in the strongly bound regime. Additionally, perturbative corrections could be introduced to improve the agreement with variational methods, while still maintaining the computational efficiency of the finite element approach. Extending the model to include multi-body interactions, such as the effect of multiple impurities or interactions with phonons, would also be an important next step, as these factors can significantly influence excitonic behavior in real systems. Moreover, the current framework could be adapted to simulate optoelectronic devices, such as quantum dot lasers, or to investigate the effects of external fields on exciton dynamics, further broadening the applicability of this methodology in semiconductor device modeling and design. Overall, this work sets the stage for a deeper understanding of excitonic phenomena and their role in next-generation nanostructured materials and devices.

Author Contributions

Conceptualization, F.A.C, A.L.M and C.A.D.; methodology, F.A.C, A.L.M and C.A.D.; software, F.A.C; validation, F.A.C, A.L.M and C.A.D.; formal analysis, F.A.C; investigation, F.A.C; resources, F.A.C and C.A.D.; data curation, F.A.C, A.L.M and C.A.D.; writing---original draft preparation, F.A.C; writing---review and editing, F.A.C, A.L.M and C.A.D.; visualization, F.A.C; supervision, F.A.C; project administration, F.A:C; funding acquisition, F.A.C All authors have read and agreed to the published version of the manuscript.

Funding

This research was funded partially by "Convocatoria 727–Programa de Becas de Doctorado Nacionales 2015 de Colciencias"', Republic of Colombia, the project "2022-52760, Diseño de un banco de pruebas de alto rendimiento para la automatización de las pruebas mínimas de funcionamiento de la tarjeta DAPHNE en el marco de la colaboración DUNE, de la convocatoria 2021-2022 de Programática – UdeA", the project "2023-59130, Beyond the standard model in neutrino experiments, de la convocatoria FAPESP 2022" and the project "Fortalecimiento de Capacidades de Invesitgación en la Universidad de Antioquia", BPIN 2020000100039 Sistema General de Regalías, OCAD CTeI, MINCiencias, Republic of Colombia.

Acknowledgments

The authors express their acknowledge to the researchers from the GIBIC group, GICM group, "Grupo de Materia Condensada" and the Instituto de Física and the Facultad de Ciencias Exactas y Naturales of the Universidad de Antioquia, Medellín - Colombia who supported the development of this research project. Also, F. A. Castaño gratefully acknowledges the support received from the "Convocatoria 727 – Programa de Becas de Doctorado Nacionales 2015 de Colciencias" in the Republic of Colombia.

Conflicts of Interest

The authors declare no conflict of interest. The funders had no role in the design of the study; in the collection, analyses, or interpretation of data; in the writing of the manuscript; or in the decision to publish the results.

References

Bastard, G.; Mendez, E. E.; Chang, L. L.; Esaki, L. (1982). Exciton binding energy in quantum wells. *Physical Review B*, 26(4), 1974–1979. https://doi.org/10.1103/physrevb.26.1974

Bauer, G. E. W.; Ando, T. (1988). Theory of magnetoexcitons in quantum wells. *Physical Review B*, 37(6), 3130(R). https://doi.org/10.1103/PhysRevB.37.3130

Belov, P. A.; Arkhipov, R. M. (2023). Formation of the stopped polarization pulse in a rectangular quantum well. *Micro and Nanostructures*, 180, 207607. https://doi.org/10.1016/j.micrna.2023.207607

Belov, P. A.; Khramtsov, E. S. (2017). The binding energy of excitons in narrow quantum wells. *Journal of Physics: Conference Series*, 816, 012018. https://doi.org/10.1088/1742-6596/816/1/012018

Blancon, J.-C.; Stier, A. V.; Tsai, H.; Nie, W.; Stoumpos, C. C.; Traoré, B.; Pedesseau, L.; Kepenekian, M.; Katsutani, F.; Noe, G. T.; Kono, J.; Tretiak, S.; Crooker, S. A.; Katan, C.; Kanatzidis, M. G.; Crochet, J. J.; Even, J.; Mohite, A. D. (2018). Scaling law for excitons in 2D perovskite quantum wells. *Nature Communications*, 9(1), 2254. https://doi.org/10.1038/s41467-018-04659-x

Christol, P.; Lefebvre, P.; Mathieu, H. (1993). Fractional-dimensional calculation of exciton binding energies in semiconductor quantum wells and quantum-well wires. *Journal of Applied Physics*, 74(9), 5626–5637. https://doi.org/10.1063/1.354224

Chuu, D.-S.; Won, W.-L.; Pei, J.-H. (1994). Longitudinal-optical-phonon effects on the exciton binding energy in a semiconductor quantum well. *Physical Review B*, 49(20), 14554–14563. https://doi.org/10.1103/physrevb.49.14554

de Dios-Leyva, M.; Bruno-Alfonso, A.; Matos-Abiague, A.; Oliveira, L. E. (1997). Fractional-dimensional space and applications in quantum-confined semiconducting heterostructures. *Journal of Applied Physics*, 82(6), 3155–3157. https://doi.org/10.1063/1.366267

Ferreira, R.; Bastard, G. (1997). Tunnelling and relaxation in semiconductor double quantum wells. *Reports on Progress in Physics*, 60(3), 345–387. https://doi.org/10.1088/0034-4885/60/3/002

Filinov, A. V.; Riva, C.; Peeters, F. M.; Lozovik, Yu. E.; Bonitz, M. (2004). Influence of well-width fluctuations on the binding energy of excitons, charged excitons, and biexcitons in GaAs-based quantum wells. *Physical Review B*, 70(3). https://doi.org/10.1103/physrevb.70.035323

Gerlach, B.; Wüsthoff, J.; Dzero, M. O.; Smondyrev, M. A. (1998). Exciton binding energy in a quantum well. *Physical Review B*, 58(16), 10568–10577. https://doi.org/10.1103/physrevb.58.10568

Ghosh, J.; Parveen, S.; Sellin, P. J.; Giri, P. K. (2023). Recent Advances and Opportunities in Low-Dimensional Layered Perovskites for Emergent Applications beyond Photovoltaics. *Advanced Materials Technologies*, 8(17). https://doi.org/10.1002/admt.202300400

Grandjean, N.; Damilano, B.; Dalmasso, S.; Leroux, M.; Laügt, M.; Massies, J. (1999). Built-in electric-field effects in wurtzite AlGaN/GaN quantum wells. *Journal of Applied Physics*, 86(7), 3714–3720. https://doi.org/10.1063/1.371241

Greene, R. L.; Bajaj, K. K.; Phelps, D. E. (1984). Energy levels of Wannier excitons in GaAs-$Ga_{1-x}Al_xAs$ quantum-well structures. *Physical Review B*, 29(4), 1807–1812. https://doi.org/10.1103/physrevb.29.1807

Heckötter, J.; Aßmann, M.; Bayer, M. (2024). Rydberg excitons and quantum sensing. *MRS Bulletin*, 49(9), 948–957. https://doi.org/10.1557/s43577-024-00775-w

Huang, J.; Hoang, T. B.; Mikkelsen, M. H. (2016). Probing the origin of excitonic states in monolayer WSe_2. *Scientific Reports*, 6(1), 22414. https://doi.org/10.1038/srep22414

Jakubczyk, T.; Delmonte, V.; Koperski, M.; Nogajewski, K.; Faugeras, C.; Langbein, W.; Potemski, M.; Kasprzak, J. (2016). Radiatively Limited Dephasing and Exciton Dynamics in $MoSe_2$ Monolayers Revealed with Four-Wave Mixing Microscopy. *Nano Letters*, 16(9), 5333–5339. https://doi.org/10.1021/acs.nanolett.6b01060

Leavitt, R. P.; Little, J. W. (1990). Simple method for calculating exciton binding energies in quantum-confined semiconductor structures. *Physical Review B*, 42(18), 11774–11783. https://doi.org/10.1103/physrevb.42.11774

Leavitt, R. P.; Littlejohn, M. A. (2015). Excitons in square quantum wells: microscopic modeling and experiment. *ArXiv Preprint*, arXiv:1508.00480.

Riva, C.; Peeters, F. M.; Varga, K. (2000). Excitons and charged excitons in semiconductor quantum wells. *Physical Review B*, 61(20), 13873–13881. https://doi.org/10.1103/physrevb.61.13873

Turner, D. B.; Nelson, K. A.; Cundiff, S. T. (2012). Persistent exciton-type many-body interactions in GaAs quantum wells measured using two-dimensional optical spectroscopy. *Physical Review B*, 85(20), 201303(R). https://doi.org/10.1103/PhysRevB.85.201303

Wang, F.; Wang, Y.; Liu, Y.-H.; Morrison, P. J.; Loomis, R. A.; Buhro, W. E. (2015). Two-Dimensional Semiconductor Nanocrystals: Properties, Templated Formation, and Magic-Size Nanocluster Intermediates. *Accounts of Chemical Research*, 48(1), 13–21. https://doi.org/10.1021/ar500286j

Wang, G.; Marie, X.; Gerber, I.; Amand, T.; Lagarde, D.; Bouet, L.; Vidal, M.; Balocchi, A.; Urbaszek, B. (2015). Giant Enhancement of the Optical Second-Harmonic Emission of WSe_2 Monolayers by Laser Excitation at Exciton Resonances. *Physical Review Letters*, 114(9), 097403. https://doi.org/10.1103/PhysRevLett.114.097403

Yücel, M. B.; Sari, H.; Duque, C. M.; Duque, C. A.; Kasapoglu, E. (2022). Theoretical Study of the Exciton Binding Energy and Exciton Absorption in Different Hyperbolic-Type Quantum Wells under Applied Electric, Magnetic, and Intense Laser Fields. *International Journal of Molecular Sciences*, 23(19), 11429. https://doi.org/10.3390/ijms231911429

Zhong, X.; Ni, X.; Sidhik, S.; Li, H.; Mohite, A. D.; Brédas, J.; Kahn, A. (2022). Direct Characterization of Type-I Band Alignment in 2D Ruddlesden–Popper Perovskites. *Advanced Energy Materials*, 12(45). https://doi.org/10.1002/aenm.202202333